Supplementary Information

Protonation of key acidic residues is critical for the K^+-selectivity of the Na/K pump

Haibo Yu[1,2]*, Ian Rathealβ, Pablo Artigas*[3] *and Benoît Roux*[1]

[1] *Department of Biochemistry and Molecular Biology, University of Chicago, Chicago, IL 60637, USA.*

[2] *Present address: School of Chemistry, University of Wollongong, NSW 2522, Australia.*

[3] *Department of Cell Physiology and Molecular Biophysics, Texas Tech University Health Sciences Center, Lubbock, TX 79430, USA.*

Correspondence should be addressed to Benoît Roux: roux@uchicago.edu

Supplementary Methods

Atomic systems and simulations

All the molecular dynamics (MD) free energy perturbation (FEP) simulations were carried out using the program CHARMM [1]. The list of all simulations is given in Supplementary Table **1**.

Supplementary Table 1: **Summary of all MD simulations**

Systems	Binding site residues				Simulation time (ns)	
					Equilibration	FEP/MD
A	E334-	E786-	D811-	D815-	10 (10)	6.6 (6.6)
B	E334	E786	D811-	D815	20 (20)	6.6 (6.6)
B'	E334	E786	D811-	D815		55
B"	E334	E786	D811-	D815		55+60+60
C	E334	E786	D811-	D815-	5	6.6
D	E334-	E786	D811-	D815	5	6.6
E	E334	E786-	D811-	D815	5	6.6
F	E334	E786	D811-	D815N	10	6.6
G	E334Q	E786	D811-	D815	10	6.6
H	E334	E786Q	D811-	D815	10	6.6

The "-" symbol denotes that the acidic residues are deprotonated. The simulation B' is an unrestrained FEP/MD calculation of the pKa of Asp815 (55 ns). The simulation B" is a restrained FEP/MD + umbrella sampling calculation of the pKa of Asp815 (60 ns for each of the two PMF calculations with the RMSD restraining potentials with protonated or deprotonated Asp815). All other simulations were started from the well-equilibrated structure in simulation B, which is based on the 2ZXE crystal structure [2]; simulations based on the 3B8E structure [3] are given in parentheses.

The FEP/MD simulations probing the K^+/Na^+ selectivity (Supplementary Table **1**, simulations A, B, C, D, E, F, G, H) were carried out for 11 evenly spaced λ windows with 600 ps of simulation per window for a total of 6.6 ns. To avoid a straightforward truncation of the large system, which would lead to inaccurate results due to the neglect of long-range electrostatic effects, the influence of the surrounding outer region on the atoms of the inner region was incorporated with the General Solvent Boundary Potential (GSBP) in the form of a solvent-shielded static field, and a solvent-induced reaction field [4]. The reaction field caused by changes in charge distribution of the dynamic inner region is expressed in terms of a basis set expansion of the charge density within the inner simulation region. The basis set coefficients correspond to generalized electrostatic multipoles. Here, a basis set of 400 spherical harmonic functions was used. The solvent-shielded static field and the reaction field matrix, representing the couplings between the generalized multipoles, were both invariant with respect to the configuration of the explicit atoms in the inner simulation region. They were calculated once with finite-difference Poisson-Boltzmann (PB), assuming dielectric constants of 1.0 inside the protein, immersed in a solvent with a dielectric constant of 78.5. The atomic Born radii for protein atoms

used to setup the dielectric boundaries in the PB calculations were determined by free energy simulations with explicit solvent [5]. The water molecules within the inner region are confined by a non-polar cavity potential to prevent entry into the surrounding dielectric continuum.

The CHARMM27 force field was used for the protein structure [6]. The water molecules were represented by the TIP3P model [7]. Following a strategy established in previous work [8], the Lennard-Jones parameters were optimized to yield accurate solvation free energies. Briefly, the Lennard-Jones parameters used in all the simulations were Emin = -0.0469 kcal/mol and Rmin/2 = 1.41075 Å for the Na^+ ion, and Emin = -0.0870 kcal/mol and Rmin/2 = 1.76375 Å for the K^+ ion. Furthermore, the pair-specific Lennard-Jones parameters (NBFIX) with Emin = -0.1021763 kcal/mol and Rmin = 3.64275 Å were used for the Na^+-carbonyl oxygen interaction, and Emin = -0.0750200 kcal/mol and Rmin = 3.2975 Å were used for the K^+-carbonyl oxygen interaction.

The reduced system was hydrated with 20 cycles comprising 5000 steps of Grand Canonical Monte Carlo [9] and 100 ps of Langevin MD at 298.15 K with 1 fs time step. A friction constant corresponding to a relaxation time of 5 ps was applied to all the non-hydrogen atoms. The bonds involving hydrogens and the TIP3 water geometry were kept rigid using SHAKE [10]. All explicit electrostatic interactions beyond 12 Å in the inner region were treated on the basis of dipolar and quadrupolar expansions using the Extended Electrostatic method (EXTE ELEC) [11]. This treatment of the non-bonded interactions reduces the computational time by about a factor of 2 relative to a no-cutoff scheme for the entire inner region while avoiding the artifacts caused by a truncation of electrostatic interactions. The two reported X-ray structures of the Na/K pump were used the calculations (PDB id 3B8E [3] and PDB id 2ZXE [2]). The residue numbering in different organisms is given in Supplementary Table **2** for convenience.

Supplementary Table 2: **Corresponding residue numbers for different Na/K pump**

Residues	Species and PDB identifier		
	spiny dogfish 2ZXE	pig 3B8E	human α_2
Asp	811	804	808
Asp	815	808	812
Glu	334	327	331
Glu	786	779	783
Asp	933	926	930
Glu	961	954	958

Explicit solvent pKa calculations

To overcome the known limitations of pKa calculations based on the continuum electrostatics protocol, we carried out additional pKa shift calculations of Asp815 with explicit solvent simulations. The pKa shift is defined as $\Delta\mathrm{pKa} = \Delta\Delta G/(2.303k_{\mathrm{B}}T)$, with $\Delta\Delta G = [\Delta G_{\mathrm{protein}} - \Delta G_{\mathrm{model}}]$, where $\Delta G_{\mathrm{model}}$ refers to the free energy of deprotonation of an isolated residue in bulk solution. For $\Delta G_{\mathrm{protein}}$, two different approaches were adopted. The first approach, unrestrained FEP/MD, is based on a direct unbiased alchemical perturbation of a protonated Asp into a deprotonated Asp. In this case, 11 evenly spaced windows between 0 and 1 were adopted in the current simulations and the results are shown as a function of the simulation time in Supplementary Figure **1**a (in red). However, an unrestrained FEP/MD approach sometimes suffers from convergence problems due to the very different conformations of the residue of interest. This can be especially problematic for buried residues [12]. Here, difficulties can occur because of the strong interactions of the residues being protonated or deprotonated. To address this problem, we also computed the pKa shift using a second approach, restrained FEP/MD with umbrella sampling (US). The method, which combines alchemical perturbation performed with a restraining potential together with umbrella sampling simulations, is similar to the ideas developed for absolute binding free energy calculations [13]. Key to this method is the potential of mean force (PMF) for the conformation of the binding site. Here, the PMF is calculated in terms of ζ, the root-mean-square deviation (RMSD) of the binding site with respect to a reference conformation (a structure from the equilibrium simulation was used). The free energy difference is written as,

$$e^{-\beta[G(1)-G(0)]} = e^{-\beta[G(1)-G(0)]_{\zeta_1}} \times \frac{\int d\zeta e^{-\beta u_{\mathrm{c}}(\zeta)} e^{-\beta W_0(\zeta)} / \int d\zeta e^{-\beta W_0(\zeta)}}{\int d\zeta e^{-\beta u_{\mathrm{c}}(\zeta)} e^{-\beta W_1(\zeta)} / \int d\zeta e^{-\beta W_1(\zeta)}}. \quad (1)$$

where $[G(1) - G(0)]_{\zeta_1}$ is the alchemical free energy calculated in the presence of the restraining potential $u_{\mathrm{c}}(\zeta)$ keeping the binding site around its conformation when the residue is protonated, and $W_1(\zeta)$ and $W_0(\zeta)$ are the PMFs with the residue protonated or deprotonated, respectively. The PMFs were calculated with umbrella sampling simulations [14, 15] (shown in Supplementary Figure **1**b) started from the configuration at the end of simulation B as a starting point. With these two approaches, the predicted pKa up-shifts are 6.7 (free FEP/MD) and 5.3 (restrained FEP/MD + US), respectively. The natural pKa of the aspartic side chain is 4.1 [16], resulting in an estimated pKa of about 10.8 and 9.4 for Asp815, respectively. Both methods (simulations B' and B") indicate that Asp815 should be protonated at physiological conditions. In the current GSBP setup, the dielectric constant for the protein interior is set to 1.0. It is likely that a more realistic treatment of the protein and lipids environment would provide a more accurate description of the pKa shift of Asp815.

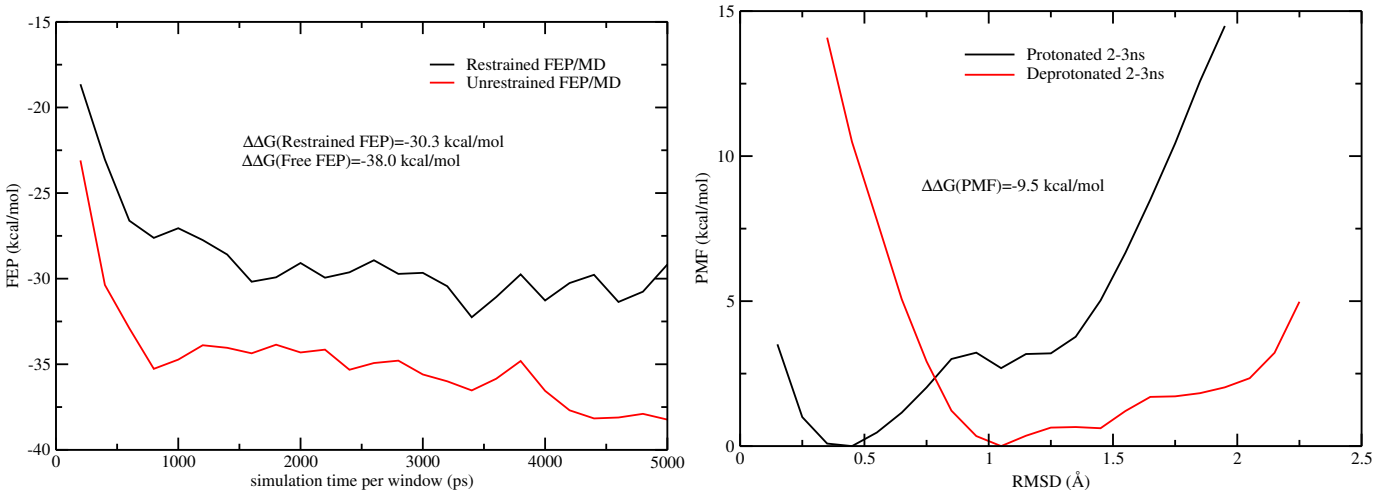

Supplementary Figure 1: pKa calculation with explicit solvent simulations. The predicted free energies of deprotonation of Asp815 are -38.0 kcal/mol in unrestrained FEP/MD and -39.8 kcal/mol in restrained FEP/MD with umbrella sampling, in comparison to -47.1 kcal/mol, the free energy of deprotonation for an isolated Asp molecular in a 18 Å solvent boundary condition setup [17]. Combining these results yields a pKa "shift" of (-38.0+47.1)/(2.3 $k_{\mathrm{B}}T$) = 6.7 and (-39.8+47.1)/(2.3 $k_{\mathrm{B}}T$) = 5.3 for the two methods, respectively. (left) Free energy perturbations in unrestrained FEP/MD and in restrained FEP/MD with umbrella sampling; (right) The PMF contributions from the umbrella sampling.

Stability of the binding sites and ion coordination

Equilibrium simulations were carried out to study the effects of the protonation states of the key acidic residues on the stabilities of the cation binding sites. The snapshots taken from the equilibrium simulations with the four acidic residues adopting the predicted protonation states (simulation B) or being deprotonated (simulation A) are shown in Supplementary Figure. **2**. The heavy atom room-mean-square deviations (RMSD) from the reference X-ray structure in the simulations where the four acidic residues adopted the predicted protonation states (simulation B) are shown in Supplementary Figure **3**. These results demonstrated that the protonation states have a considerable impact on the stabilities of the K^+ binding sites.

The radial distribution function (RDF) and the coordination number at the two cation binding sites (simulation B) are shown in Supplementary Figure **4**. The coordination numbers for Site I and Site II within 3.5 Å are 6.3 and 7.4, respectively, with 1.4 and 0.0 being water oxygen atoms.

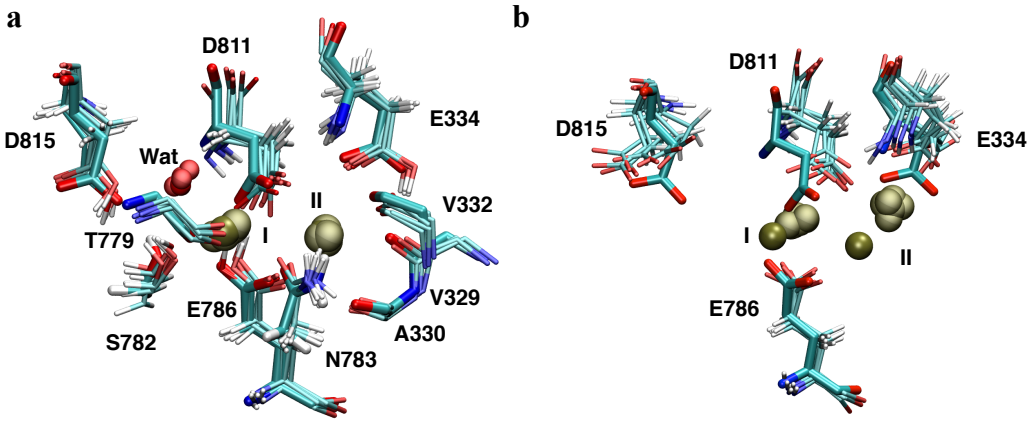

Supplementary Figure 2: Superposition of the X-ray structure and snapshots from the simulations based on the crystal structure 2ZXE (drawn with thicker lines and ions darker). **a.** Snapshots taken at 5ns, 8ns, 11ns, 14ns, 17ns, and 20ns with the protonation states of the binding site residues assigned according to the theoretical prediction (simulation B); The average heavy-atom RMSD are (in Å) 0.5 for Glu334, 0.4 for Glu786, 0.8 for Asp811, and 0.8 for Asp815. **b.** Snapshots taken at 5ns, 6ns, 7ns, 8ns, 9ns, and 10ns with the binding site residues deprotonated; The average heavy-atom RMSD are (in Å) 1.7 for Glu334, 1.0 for Glu786, 2.2 for Asp811, and 1.5 for Asp815 (simulation A).

For comparison, equilibrium simulations were carried out to investigate the effects of the protonation states of Glu334 (simulation D), Glu786 (simulation E), and Asp815 (simulation C) on the stability of the binding sites. The simulations were carried out by deprotonating the specific residue while keeping the proper protonation states of the other two residues. The radial distribution function between K^+ and the coordinating oxygen atoms (RDF) and the coordination number at the two cation binding sites of the Na/K pump from the equilibrium simulations are shown in Supplementary Figure **5** and **6**. In all simulations (C, D, and E), the minimal distances between K^+ and oxygen atoms become shorter due to the stronger interactions with the negatively charged carboxylate groups, while the binding sites become water accessible. All the binding

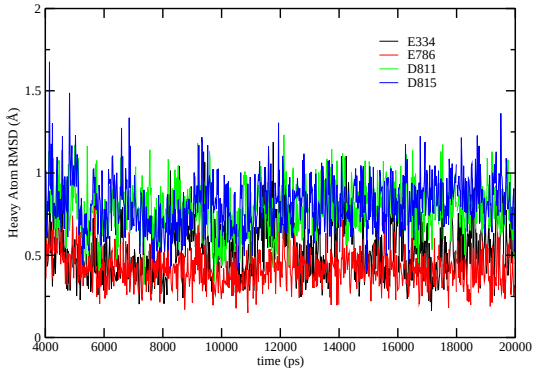

Supplementary Figure 3: The heavy atom room-mean-square deviations (RMSD) for Glu334, Glu786, Asp811 and Asp815 relative to the reference X-ray structure (2ZXE) in simulation B.

sites become Na^+ selective except Site II when Asp815 deprotonated. Deprotonation of D815 leads to a partial loss of selectivity (Table 2, simulation C: site I is non-selective while site II remains selective). Further analysis indicates that when Asp815 is deprotonated, the site I becomes more water accessible (see figure **5**e and **6**e) The coordination environment analysis indicates that there are 2.6 water molecules within the first coordination shell in simulation C in contrast to 1.4 in simulation B. The total coordination number increased

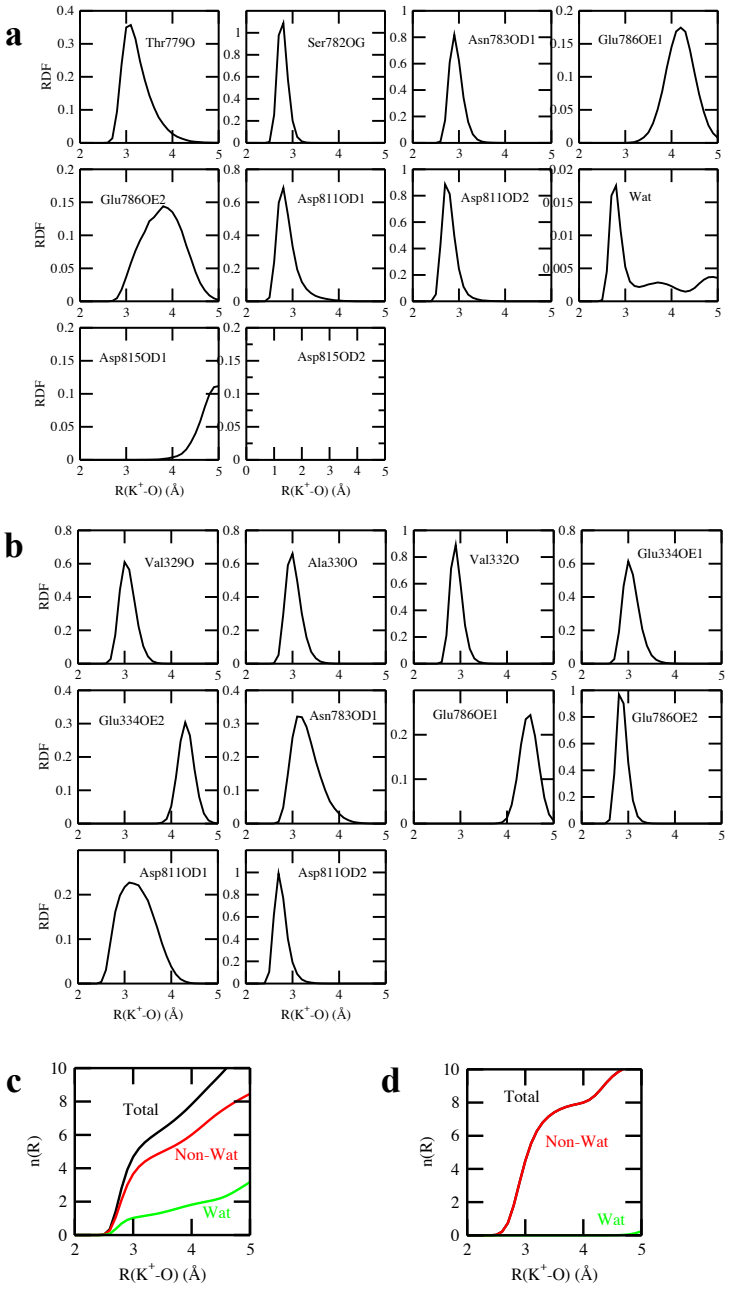

Supplementary Figure 4: The radial distribution function (RDF) between the K^+ ion and the coordinating oxygen atoms and the coordination number, $n(R)$, as a function of the cutoff distance R for the two binding sites from the equilibrium simulations B (Table **1**). **a.** The RDF for the K^+ ion in the site I; **b.** The RDF for the K^+ ion in the site II; **c.** The n(R) for the K^+ ion in the site I; **d.** The n(R) for the K^+ ion in the site II.

from 6.3 to 7.0.

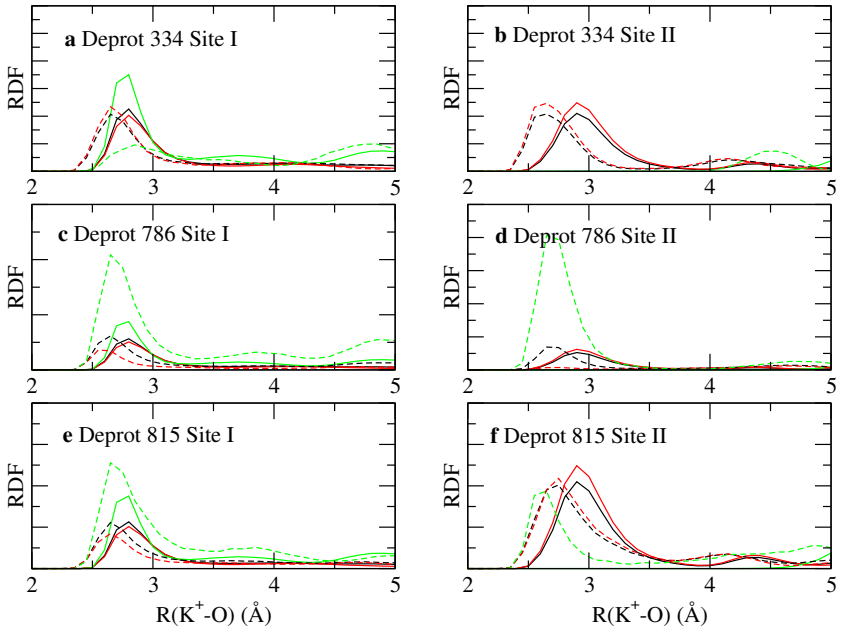

Supplementary Figure 5: The radial distribution function (RDF) between the K^+ ion and the coordinating oxygen atoms the two binding sites of the Na/K pump from the equilibrium simulations in which Glu334 (simulation D; a,b) or Glu786 (simulation E; c,d) or Asp815 (simulation C; e,f) were deprotonated. Solid line: the protonation states were assigned according to the theoretical prediction (simulation B); Dashed line: one of the residues was deprotonated. Black: all oxygen atoms; Red: non-water oxygen atoms; Green: water oxygen atoms.

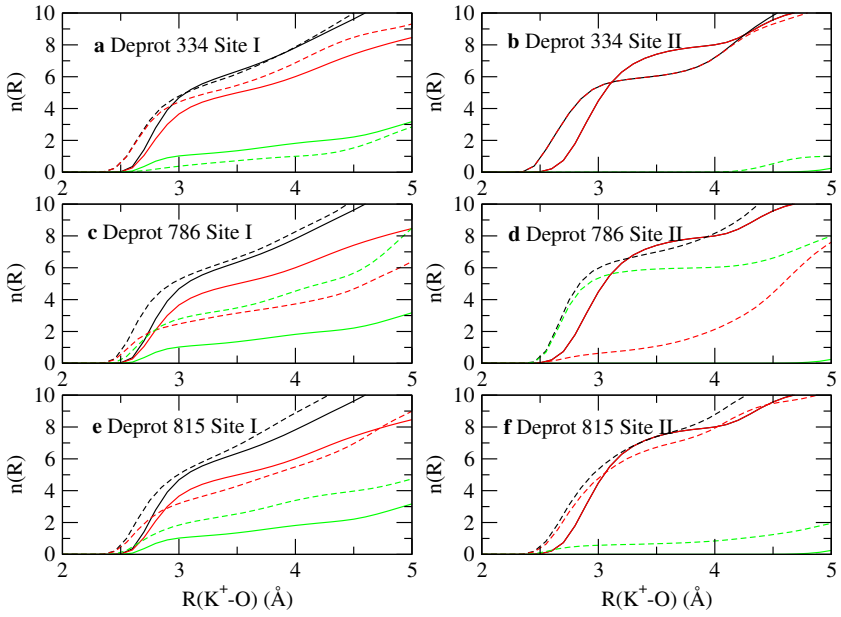

Supplementary Figure 6: The number of coordinating oxygen atoms $n(R)$ around the K^+ ions as a function of the cutoff distance. Shown are the results for the two binding sites of the Na/K pump from the equilibrium simulations in which Glu334 (simulation D; a,b) or Glu786 (simulation E; c,d) or Asp815 (simulation C; e,f) were deprotonated. Solid line: the protonation states were assigned according to the theoretical prediction (simulation B); Dashed line: one of the residues was deprotonated. Black: all oxygen atoms; Red: non-water oxygen atoms; Green: water oxygen atoms.

Reduced binding site models

To assess the robustness of the present results, additional computations based on simplified reduced models retaining the essential elements of the binding sites were carried out. Analysis of simplified binding site models can provide a useful theoretical route to probe and dissect the key factors governing ion selectivity [8, 18, 19, 20, 21]. Here, the reduced model of the K^+-selective binding sites of the Na/K pump was constructed by including the residues within 5 Å around the bound ions. The procedure follows a theoretical formulation of reduced models of selective binding sites, which was recently elaborated to clarify the molecular determinants of ion selectivity in protein binding sites [21]. On the basis of this analysis, it was concluded that architectural stiffness provided by the surrounding protein structure serves to enhance rather than oppose the selectivity that is already emerging in the confined microdroplet regime [21]. The latter corresponds to an inherent trend that is robustly set by the number and type of ion coordinating ligands. Reverting the inherent trend is possible, but only by making the local structure extremely stiff, leading to conditions that may be difficult to be realistically achieved for most flexible biological macromolecules. Stabilizing the local geometry to build upon the inherent selectivity set by the number and type of ion coordinating ligands appears to be one of the key *design principles* of ion-selective binding sites in proteins and other biological macromolecules.

The binding selectivity is governed by the relative free energy $\Delta\Delta G_{ij} = \Delta G^{\rm site}_{ij} - \Delta G^{\rm bulk}_{ij}$, where $\Delta G^{\rm bulk}_{ij} = [G^{\rm bulk}_i - G^{\rm bulk}_j]$ is the free energy difference between ion i and j in the bulk solvent, and $\Delta G^{\rm site}_{ij} = [G^{\rm site}_i - G^{\rm site}_j]$ is the free energy difference between ion i and j in the binding site. We construct a reduced subsystem comprising only the bound ion and the n most important ligands that are directly participating in the binding site, and express the relative free energy of ions i and j as in the binding site as,

$$\begin{aligned} e^{-\beta\Delta G^{\rm site}_{ij}} &= \frac{\int_{\rm site} d\mathbf{X}\, d\mathbf{Y}\; e^{-\beta U_i(\mathbf{X},\mathbf{Y})}}{\int_{\rm site} d\mathbf{X}\, d\mathbf{Y}\; e^{-\beta U_j(\mathbf{X},\mathbf{Y})}} \\ &= \frac{\int_{\rm site} d\mathbf{X}\; e^{-\beta[U^{\rm il}_i(\mathbf{X}) + U^{\rm ll}(\mathbf{X}) + \Delta W^{\rm site}(\mathbf{X})]}}{\int_{\rm site} d\mathbf{X}\; e^{-\beta[U^{\rm il}_j(\mathbf{X}) + U^{\rm ll}(\mathbf{X}) + \Delta W^{\rm site}(\mathbf{X})]}} \end{aligned} \tag{2}$$

where $U^{\rm il}$ and $U^{\rm ll}$ represent the ion-ligand and ligand-ligand interactions, respectively, and $\Delta W^{\rm site}(\mathbf{X})$ is an effective potential of mean force (PMF) that incorporates all the influence of the rest of the system (protein, membrane and solvent). This PMF is separated into two distinct contributions, called "confinement" and "geometric", $\Delta W^{\rm site} = \Delta W^{\rm site}_{\rm c} + \Delta W^{\rm site}_{\rm g}$. The first contribution, $\Delta W^{\rm site}_{\rm c}$, accounts for the generic effect of the protein structure surrounding the reduced subsystem imposing an upper limit on the fluctuations of the bound ion and its coordinating ligands. This is constructed from Heaviside functions. The second contribution, $\Delta W^{\rm site}_{\rm g}$, accounts for the remaining architectural forces from the surrounding protein that enforce a precise

geometry to the atoms of the inner region. This is constructed from harmonic potentials,

$$\Delta W_{\rm g}^{\rm site}(\mathbf{X};\lambda_{\rm g}) = \lambda_{\rm g}\sum_k (\mathbf{r}_k - \bar{\mathbf{r}}_k)^2 \tag{3}$$

where $\lambda_{\rm g}$ has the dimension of a harmonic spring constant (kcal/mol/Å^2), and its optimal value should be determined self-consistently by performing averages to match the reference values extracted from all-atom MD with ion i and j.

The range of confinement of the protein atoms in the reduced model (R_k in Eq. 3 in Ref. [21]) was extracted from 2 ns well equilibrated MD simulations under the GSBP condition. The variables for the confinements include 78 Cartesian atomic positions. Geometric structural forces were introduced in the form of a harmonic restraining potential with respect to the configurations optimized from the X-ray structure of the Na/K pump [2]. Selectivity for K^+ and Na^+ was calculated from more than 4 ns FEP/MD simulations of the reduced model, post-processed using the weighted histogram analysis method [14, 15]. Here, a clear conclusion can be drawn. If the acidic residues are deprotonated, both cation binding sites become unambiguously Na^+ selective over K^+. In the case of site I, the incorrect selectivity cannot be reversed, even when infinitely increasing the stiffness of the local structure. In the case of site II, the incorrect selectivity can be reversed, but only if the structural stiffness is increased beyond what can be realistically achieved for a protein. The trends noted in the FEP/MD simulations are robust and are not overly sensitive to slight structural changes because they are inherently governed by the number and chemical nature of the coordinating ligands rather than by a precise molecular geometry.

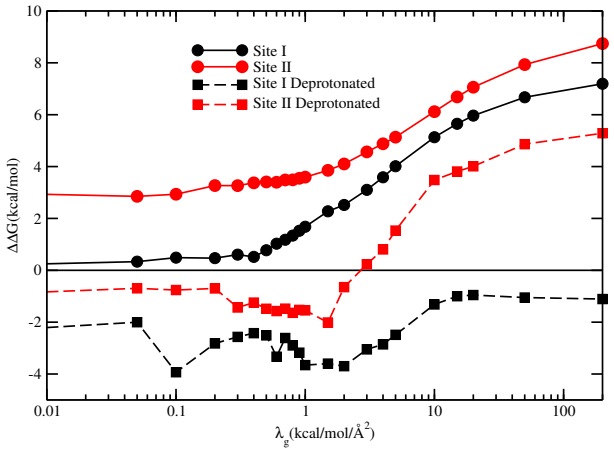

Supplementary Figure 7: Ion selectivity $\Delta\Delta G_{\rm Na,K}$ as a function of the geometric force constant $\lambda_{\rm g}$ calculated from FEP/MD simulations of the reduced models of the Na/K pump. Solid lines refer to the constructed reduced models where the four acidic residues adopt the predicted protonation states (simulation B); Dashed lines refer to the constructed reduced models where all four acidic residues are deprotonated (simulation A).

Apparent selectivity and pH

Consider one ionizable binding site, which can be either protonated or deprotonated, that can be occupied by a K^+ or a Na^+ ion. The effective pH-dependent selectivity of the site for K^+ over Na^+ represents an average over all possible ionization states,

$$\Delta\Delta G^{(\mathrm{eff})}_{\mathrm{Na,K}} = -k_{\mathrm{B}}T \ln \left[\frac{e^{-\beta\Delta G^{(\mathrm{d})}_{\mathrm{Na}}} + e^{-\beta\Delta G^{(\mathrm{p})}_{\mathrm{Na}}}}{e^{-\beta\Delta G^{(\mathrm{d})}_{\mathrm{K}}} + e^{-\beta\Delta G^{(\mathrm{p})}_{\mathrm{K}}}} \right] \tag{4}$$

where the various ΔG^s_i represent the free energies with either Na^+ or K^+ bound to a protonated (p) or deprotonated (d) site (all the free energies are shifted by the solvation free energy of the ions in bulk water). With a simple re-arrangement, the effective selectivity can be expressed as

$$\Delta\Delta G^{(\mathrm{eff})}_{\mathrm{Na,K}} = -k_{\mathrm{B}}T \ln \left[\left(1 - P^{(\mathrm{p})}\right) e^{-\beta\Delta\Delta G^{(\mathrm{d})}_{\mathrm{Na,K}}} + P^{(\mathrm{p})} e^{-\beta\Delta\Delta G^{(\mathrm{p})}_{\mathrm{Na,K}}} \right] \tag{5}$$

where $\Delta\Delta G^{(\mathrm{d})}_{\mathrm{Na,K}}$ is equal to $[\Delta G^{(\mathrm{d})}_{\mathrm{Na}} - \Delta G^{(\mathrm{d})}_{\mathrm{K}}]$, $\Delta\Delta G^{(\mathrm{p})}_{\mathrm{Na,K}}$ is equal to $[\Delta G^{(\mathrm{p})}_{\mathrm{Na}} - \Delta G^{(\mathrm{p})}_{\mathrm{K}}]$, and $P^{(\mathrm{p})}$ is the probability of finding the site protonated when a K^+ is bound in the site,

$$P^{(\mathrm{p})} = \frac{e^{-\beta G^{(\mathrm{p})}_{\mathrm{K}}}}{e^{-\beta G^{(\mathrm{d})}_{\mathrm{K}}} + e^{-\beta G^{(\mathrm{p})}_{\mathrm{K}}}} = \frac{10^{[\mathrm{pKa-pH}]}}{1 + 10^{[\mathrm{pKa-pH}]}} \tag{6}$$

The pKa of the site is defined with a bound K^+, as in the X-ray structure. This analysis can be used to understand the effect of pH on the effective selectivity of a site. For example, let us consider the site I. With a protonated Asp815, the site displays a selectivity of +1.9 kcal/mol for K^+ over Na^+. but with a deprotonated Asp815, the relative free energy is -1.5 kcal/mol and the site becomes selective for Na^+ over K^+. The pKa of Asp815 is up-shifted to a value around 9.4 according the FEP/MD. Experimentally, the pH is varied from 7.6 to 9.6, which yields a decrease in apparent selectivity for K^+. Using these values, we plot the curve shown in Supplementary Figure **8**. It is observed that there is loss of selectivity as the pH is increased, but it is less than the difference of 3.4 kcal/mol between the two extreme values. Thus, the observed change in relative free energy reflects a weighted average of two ionization states.

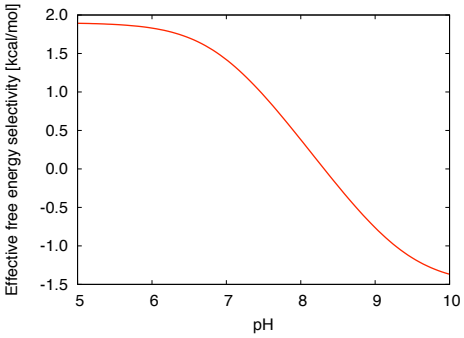

Supplementary Figure 8: Effect of pH on the effective (apparent) selectivity $\Delta\Delta G^{(\mathrm{eff})}_{\mathrm{Na,K}}$ using the values calculated from FEP/MD.

Effects of other titratable residues

The effects of the protonation states of other titratable resides were investigated by examine the change of the electrostatic potential at the cation binding sites (Supplementary Figure). We focused on the residues which have a predicted pKa within the range of 5.5 and 8.5 and are likely to switch the protonation states under physiological conditions. The calculations were carried out with the PBEQ module in CHARMM. The system was mapped onto a grid and the Poisson-Boltzmann equation were solved numerically with finite-difference. The orientations of Na/K-pump in membranes were estimated using the OPM database (http://opm.phar.umich.edu/). The membrane was represented as a low-dielectric slab (ϵ_m = 2.0) of 31.9 Å thickness surrounding a cylinder of radius of 30 Å to accommodate the transmembrane region of the pump. The calculations was performed in two steps, first using a coarse grid spacing of 2.4 Å followed by a focusing around the main region with a finer grid spacing of 0.25 Å centered at the middle point of the two K^+ binding sites. The dielectric constants of the protein was set to 4.0 and the salt concentration was set to 0.150 M. The identified residues are some distance away from the bound ions and their interactions with the ions are expected to be mainly electrostatic. The induced electrostatic potential change at the binding sites due to the change of the protonation states are fairly small and thus we can conclude that these residues have a small effect on the K^+ selectivity at the E2·Pi state. Of significance, there are also three histidines near the binding sites (His290, His 293, His919). Their pKa's have low values, indicating that they should remain deprotonated and neutral in the E2P state, but some of those histidines might be able to accept a proton in the E1 state.

Supplementary Table 3: **The effect of the protonation states of the titratable Asp and Glu on the electrostatic potential at the K^+ binding sites.**

Residue ID	pKa[a]	Distance (Å) [b]	$\Delta\Delta E$ (kcal/mol) [c]
α subunit			
Asp42	6.8	63.5	-0.0002606
Asp189	5.8	69.7	-0.0001268
Asp202	7.5	61.1	-0.0005304
Asp376	8.0	45.7	-0.0080921
Asp900	6.1	33.5	-0.0548275
Glu221	6.7	55.1	-0.0016466
Glu362	8.3	23.5	-0.2542129
Glu365	6.4	24.0	-0.3397300
Glu494	5.6	85.7	-0.0000000
Glu550	6.1	62.5	-0.0002813
Glu764	5.5	26.3	-0.0985097
Glu875	6.6	28.7	-0.1028175
Glu960	5.7	17.3	-0.1985114
Glu1020	5.8	22.2	-0.0733870
β subunit			
Asp291	5.6	33.7	-0.0251203
Glu200	5.5	57.7	-0.0004405
Glu298	5.6	42.3	-0.0078477

[a] The pKa values were obtained with PROPKA 3.0. [b] The distance refers to those between the C_α atom and the Site I. [c] The electrostatic potential differences between the protonated and deprotonated states at the mid point of the two K^+ binding sites.

Simulation of mutants

In order to further probe the importance of the protonation states of the binding site residues, three additional FEP/MD simulations were carried out for the three mutants, D815N (simulation F), E334Q (simulation G), E786Q (simulation H). Such FEP/MD simulations for the mutants are more uncertain than those based on the wild-type crystal structure because of the need to construct the new side chain in a proper orientation. In the setup, the -NH group of the neutral side chain (Asn or Gln) was placed at the protonated -OH group of the acidic wide-type residue (Asp or Glu) starting from a well equilibrated wild-type configuration (simulation B). Atomic positional harmonic restraining potentials were applied to the heavy atoms with a force constant decreasing from 4.0 kcal/mol/Å^2 to zero over a period of 1 ns and then the systems were equilibrated of 9 ns. For the K^+/Na^+ selectivity calculations, FEP/MD simulations were carried out for 11 evenly spaced λ windows with 600 ps of simulation per window for a total of 6.6 ns. (Table 1, simulations G, H and F). In interpreting the results, it is important to note that the calculated relative free energies $\Delta\Delta G_{\mathrm{Na,K}}$ for the mutants do not provide any information about the changes in the absolute affinity of those ions for the binding sites. In the D815N mutant (F), the effects introduced by the mutation on K^+ selectivity is rather limited. This might be due to the fact that the carboxylate oxygens do not participate in direct coordination of Site I (Supplementary Figure **4 a**) and that the perturbation introduced by the -NH in place of the -ON group is rather small compared to the wide-type simulation (B) and the X-ray structure (2ZXE). In the E334Q (simulation G) and E786Q (simulation H), the K^+ selectivity at both Site I and Site II are considerably lost or become slightly Na^+ selective. As observed in Supplementary Figure **9**, the distortions introduced by the E334Q and E786Q are visible.

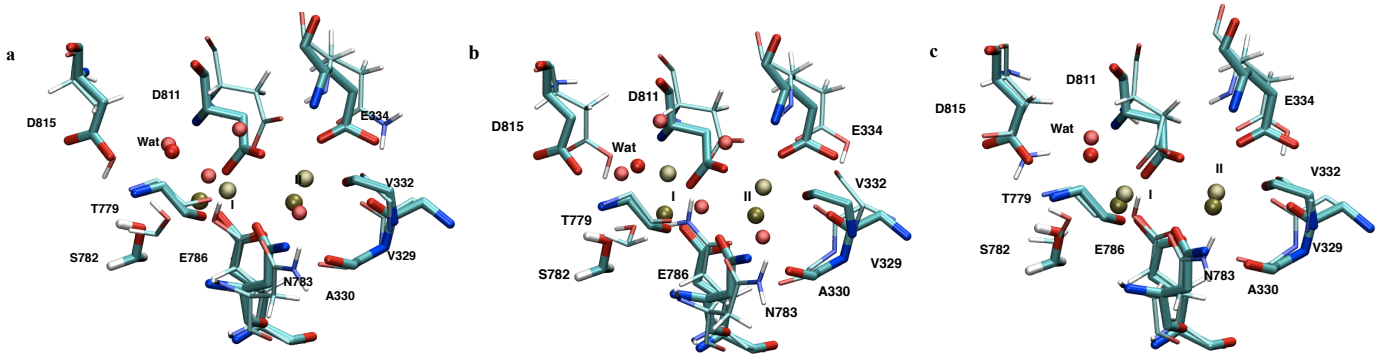

Supplementary Figure 9: The snapshots at the end of 10 ns equilibrium simulations for the mutants (thin lines): E334Q (simulation G; a), E786Q (simulation H; b) and D815N (simulation F; c), superimposed with the X-ray structure (2ZXE, thick lines).

References

[1] Brooks, B. R. *et al.* CHARMM: The biomolecular simulation program. *J. Comp. Chem.* **30**, 1545–1614 (2009).

[2] Shinoda, T., Ogawa, H., Cornelius, F. & Toyoshima, C. Crystal structure of the sodium-potassium pump at 2.4 Å resolution. *Nature* **459**, 446–U167 (2009).

[3] Morth, J. P. *et al.* Crystal structure of the sodium-potassium pump. *Nature* **450**, 1043–U6 (2007).

[4] Im, W., Berneche, S. & Roux, B. Generalized solvent boundary potential for computer simulations. *J. Chem. Phys.* **114**, 2924–2937 (2001).

[5] Nina, M., Beglov, D. & Roux, B. Atomic radii for continuum electrostatics calculations based on molecular dynamics free energy simulations. *J. Phys. Chem. B* **101**, 5239–5248 (1997).

[6] MacKerell, A. D. *et al.* All-atom empirical potential for molecular modeling and dynamics studies of proteins. *J. Phys. Chem. B* **102**, 3586–3616 (1998).

[7] Jorgensen, W. L., Chandrasekhar, J., Madura, J. D., Impey, R. W. & Klein, M. L. Comparison of simple potential functions for simulating liquid water. *J. Comp. Phys.* **79**, 926 (1983).

[8] Noskov, S. Y., Bernèche, S. & Roux, B. Control of ion selectivity in potassium channels by electrostatic and dynamic properties of carbonyl ligands. *Nature* **431**, 830–834 (2004).

[9] Woo, H. J., Dinner, A. R. & Roux, B. Grand canonical monte carlo simulations of water in protein environments. *J. Chem. Phys.* **121**, 6392–6400 (2004).

[10] Ryckaert, J. P., Ciccotti, G. & Berendsen, H. J. C. Numerical-integration of cartesian equations of motion of a system with constraints - molecular-dynamics of n-alkanes. *J. Comput. Phys.* **23**, 327–341 (1977).

[11] Stote, R. H., States, D. J. & Karplus, M. On the treatment of electrostatic interactions in biomolecular simulation. *J. Chim. Phys.-Chim. Biol.* **88**, 2419–2433 (1991).

[12] Berneche, S. & Roux, B. The ionization state and the conformation of Glu71 in the KcsA K^+ channel. *Biophys. J.* **82**, 772–780 (2002).

[13] Deng, Y. Q. & Roux, B. Computations of standard binding free energies with molecular dynamics simulations. *J. Phys. Chem. B* **113**, 2234–2246 (2009).

[14] Kumar, S., Bouzida, D., Swendsen, R., Kollman, P. & Rosenberg, J. The Weighted Histogram Analysis Method for free-energy calculations on biomolecules. I. The method. *J Comp Chem* **13**, 1011–1021 (1992).

[15] Souaille, M. & Roux, B. Extension to the Weighted Histogram Analysis Method: Combining umbrella sampling with free energy calculations. *Comp Phys Comm* **135**, 40–57 (2001).

[16] Berg, J. M., Tymoczko, J. L. & Stryer, L. *Biochemistry (5th Ed.)* (W.H. Freeman and Co., New York, 2002).

[17] Beglov, D. & Roux, B. Finite representation of an infinite bulk system - solvent boundary potential for computer-simulations. *J. Chem. Phys.* **100**, 9050–9063 (1994).

[18] Noskov, S. Y. & Roux, B. Importance of hydration and dynamics on the selectivity of the KcsA and NaK channels. *J Gen Physiol* **129**, 135–143 (2007).

[19] Noskov, S. Y. & Roux, B. Control of ion selectivity in LeuT: Two Na^+ binding sites with two different mechanisms. *J Mol Biol* **377**, 804–818 (2008).

[20] Asthagiri, D., Pratt, L. & Paulaitis, M. Role of fluctuations in a snug-fit mechanism of KcsA channel selectivity. *J Chem Phys* **125**, 24701 (2006).

[21] Yu, H., Noskov, S. Y. & Roux, B. Two mechanisms of ion selectivity in protein binding sites. *Proc. Natl. Acad. Sci. U.S.A.* **107**, 20329–20334 (2010).